75th International Astronautical Congress (IAC), Milan, Italy, 14-18 October 2024.


IAC-24-B2.IPB.31.84800

# Tradespace Analysis and Conceptual Design for a Lunar Navigation and Communication Constellation

**Matthias Kura[a]*, Alexander Zieser[a], Alexander Hoffmann[a], Falk Ramin[a], Jayanth Narra[a], Vincenzo Messina[a], Alessandro Golkar[a]**

[a] *Chair of Spacecraft Systems, Department of Aerospace and Geodesy, Technical University of Munich, Caroline Herschel Straße 100/II, 85521 Ottobrunn, Bavaria, Germany*
* Corresponding Author, matthias.kura@tum.de

**Abstract**

With an increase in Lunar exploration activity expected in the 2030s through the Artemis program as well as other governmental and private missions, infrastructure architectures are essential to enable ambitious robotic and human surface missions. Beyond the Lunar Gateway, service stations, and payload landers, high-reliability and high-accuracy navigation and communication (NAVCOM) services are a critical requirement for all Lunar surface assets. Such services enable high-precision landings, guidance for robotic/human rovers exploring unknown terrain, and a reliable and high-throughput connection to long-term human habitats. This paper aims to explore the tradespace of a constellation combining NAVCOM services around the Moon. The key research question addressed in our work is the impact of the semi-major axis, the number of orbit planes, and the number of satellites per plane of a circular frozen orbit Walker constellation on the NAVCOM performance. The figures of merit (FOMs) of the analysis include the coverage with a Geometric Dilution of Precision (GDOP) below 6, a theoretical constellation capacity, and the power flux density coverage for a Lunar orbit to Lunar surface S- and Ka-Band connection. Results indicate that minimum sets of satellites at a minimum distance from the Moon are required to fulfill global coverage and adequate performance for the NAVCOM service. In addition, it is identified that certain combinations achieve a particularly poor GDOP coverage in the equator region. From the tradespace analysis, a set of parameters is then selected for further study based on a combined performance assessment of the FOMs. Based on this selection, an exemplary NAVCOM constellation is derived, including a concept of operations, detailed navigation and communication architectures, and a satellite bus design. This 21-satellite Walker constellation can provide coverage of close to 100% with a GDOP of less than 6.0. With a regenerative communication design, it provides close to 100% surface access time for both S-and Ka-Band and a Ka-Band relay to Earth, following guidelines proposed in the LunaNet standards. This work aims to serve as a basis for further studies into Lunar communication and navigation constellations for Lunar frozen orbit Walker constellations and provides a starting point for one of the fundamental prerequisites of an extended Lunar presence.

**Keywords:** Moon, Navigation, Communication, Constellation, Tradespace

## Nomenclature

| | |
|---|---|
| $\alpha$ | Scan angle |
| $B$ | Bandwidth |
| $c$ | Speed of light |
| $C/N$ | Carrier-to-noise ratio |
| $\Delta v$ | Orbital velocity increment |
| $d$ | Distance |
| $f$ | Frequency |
| $G$ | Antenna gain |
| $G/T$ | Antenna gain-to-noise ratio |
| $J_2$ | Lunar second-order gravity harmonic coefficient |
| $k$ | Earth-Moon CR3BP parameter |
| $k_B$ | Boltzmann constant |
| $L$ | Loss |
| $\mu$ | Lunar gravitational constant |
| $M$ | Link margin |
| $n_3$ | Lunar angular velocity |
| $N_T$ | Total noise power |
| $P$ | Power |
| $R_M$ | Lunar radius |
| $\theta$ | Pointing error |
| $\theta_{3dB}$ | Beamwidth |
| $T_{sys}$ | System noise temperature |
| $(X, Y, Z)$ | Position |

## Acronyms/Abbreviations

| | |
|---|---|
| **BPSK** | Binary Phase Shift Keying |
| **CC** | Constellation Capacity |
| **CMCU** | Clock Monitoring and Control Unit |
| **EIRP** | Effective Isotropic Radiated Power |
| **ES** | Earth Surface |
| **FGUU** | Frequency Generation Upconverter Unit |
| **FOM** | Figure of Merit |
| **GDOP** | Geometric Dilution of Precision |
| **GNSS** | Global Navigation Satellite System |
| **INC** | Inclination |

| | |
|---|---|
| **LS** | Lunar Surface |
| **LO** | Lunar Orbit |
| **NAVCOM** | Navigation and Communication |
| **NOP** | Number of Planes |
| **NOS** | Number of Satellites per Plane |
| **NSGU** | Navigation Signal Generation Unit |
| **PFD** | Power Flux Density |
| **RAAN** | Right Ascension of the Ascending Node |
| **RAFS** | Rubidium Atomic Frequency Standards |
| **SMA** | Semi-major Axis |
| **SNR** | Signal-to-Noise Ratio |
| **TT&C** | Telemetry, Tracking, and Command |

## 1. Introduction

Lunar exploration is currently seeing its most significant resurgence since the Apollo era. With government programs like Artemis [1], [2] aiming to establish a long-term presence on the Moon, particularly around the Lunar South Pole, several assets in the space and ground segment are required to enable these missions. Among them, navigation and communication (NAVCOM) services are crucial to provide timing and improve rendezvous, docking, and proximity operations. Furthermore, they enable higher levels of autonomy and accuracy to increase mission safety for human and robotic missions. Therefore, previous studies have looked at suitable NAVCOM architectures for the Moon. The use of Global Navigation Satellite System (GNSS) signals in the cislunar environment and on the surface has been extensively explored [3], [4], [5], but suffers from the lack of required accuracy and, crucially, coverage of the Lunar far side [6]. Instead, several studies propose entirely new architectures [7], [8], [9], [10], [11], where constellations about Earth-Moon libration points and in frozen orbits are particularly favored. Notably, Pereira et al. [10], [11] investigated the tradespace of a GNSS constellation around the Moon through several orbital parameters and figures of merit (FOMs).

Similar to Pereira et al. [10], [11], this paper aims to explore the tradespace of a Lunar navigation constellation, however, in combination with communication services. While the number of input parameters has been reduced, introducing a communication service to the mission architecture and tradespace expands the analyses of previous studies. The first two sections cover the tradespace analysis, including the assumptions and input parameters under investigation, and the modeling of different aspects. The results for the navigation, communication, and combined performance are then presented and discussed. Based on these results, a conceptual design for a Lunar NAVCOM constellation from an architecture and system perspective is derived in Section 4. It covers the assumptions used for the design and shows the results for the constellation, including an architecture and system design for the satellites.

## 2. Tradespace Analysis

### *2.1 Assumptions, Design Vector, and Measures of Performance*

The NAVCOM constellation investigated in the tradespace aims to provide a continuous navigation and communication service for Lunar surface (LS) operations. For the communication service, two downlink connections are considered in S- and Ka-Band for high reliability and high data rate, respectively, following the standards established in the LunaNet guidelines [12]. The communication performance tradeoff focuses only on the downlink between the satellite and the LS to isolate the impact of the constellation parameters and simplify the calculation. The design space primarily considers the influence of the orbital parameters of the semi-major axis (SMA), the number of orbit planes (NOP), and the number of satellites per plane (NOS), with similar ranges as Pereira et al. [10]. The SMA is increased incrementally by the mean Lunar radius $R_M$ = 1738 km. All constellations are Walker constellations with a phasing of 1 [13]. The analysis investigates circular orbits, choosing an inclination to fulfill frozen orbit conditions [14], [15]. Table 1 summarizes the range of design parameters with a total of 900 different constellation combinations able to be constructed from the design vector.

Table 1. Design Vector Definition

| Variable | Min | Max | Increment |
|---|---|---|---|
| SMA [km] | 3476 | 17380 | 1738 |
| NOP [-] | 1 | 10 | 1 |
| NOS [-] | 1 | 10 | 1 |

Three measures of performance assess the navigation and communication capabilities of the constellation. Similar to Pereira et al. [10], the coverage with a geometric dilution of precision (GDOP) below 6 assesses the navigation performance of the constellation. The communication FOMs are a measure of theoretical maximum constellation capacity (CC) with a single link per satellite, as, for example, described by Baccelli et al. [16], and the power flux density (PFD) distribution on the surface of the Moon. Both parameters are used to indicate performance variation and only consider the link between the satellites and the Moon's surface. They do not reflect actual performance, which is considered in the conceptual design.

### *2.2 Methodology and Modelling*

This section covers the methods and assumptions for modeling the tradespace analysis. This includes the

orbital mechanics as well as the navigation and communication FOMs in the form of the CC and PFD.

### *2.2.1 Orbital Mechanics*

The initial step of the tradespace analysis is the configuration of the Walker constellation, assuming circular orbits. As pointed out before, frozen orbits are considered. For every SMA, the inclination (INC) to achieve this criterion is calculated with [15]

$$\cos(2\,INC) = -\frac{4\,SMA^5\,k\,n_3^2}{5\,J_2\,\mu\,R_M^2} - \frac{3}{5}, \tag{1}$$

where $k$ = 0.98785 is the characteristic factor in the Earth-Moon Circular Restricted Three-Body Problem, $n_3$ = 2.66e-6 rad/s is the angular velocity of the Lunar rotation, $J_2$ = 2.03e-4 is the second-order gravity harmonic coefficient of the Moon, μ = 4.903e3 km$^3$/s$^2$ is the gravitational constant of the Moon, and $R_M$ is the Lunar radius. The right ascension of the ascending node (RAAN) of the orbit planes is equally spread around the Moon. The true anomaly to get Walker constellations is calculated using NASA's General Mission Analysis Tool to get the positions of all satellites for each constellation at an initial point.

### *2.2.2 Navigation – Geometric Dilution of Precision*

The dilution of precision is a measure of the accuracy of position and time determination given a set of satellites in a constellation. One of these precision parameters is the GDOP, which is influenced by the position of the visible satellites with respect to the user. For the analysis in this paper, the GDOP coverage over 500 nearly equidistant points on the LS is calculated. The subsequent mesh is shown in Figure 1.

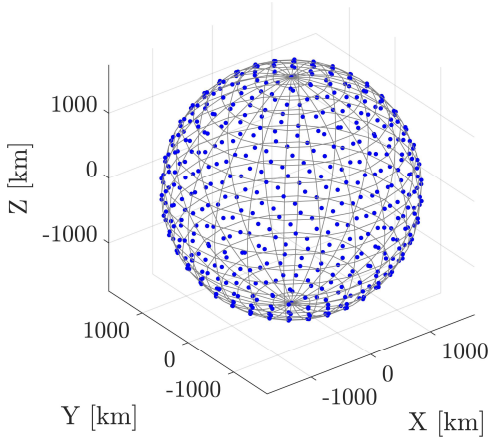


Figure 1. Surface Mesh

Given a surface point ($X_{user}$, $Y_{user}$, $Z_{user}$) and four visible satellites at positions ($X_{sat,i}$, $Y_{sat,i}$, $Z_{sat,i}$), the GDOP can be calculated by [17]

$$S = \begin{bmatrix} \frac{X_{user}-X_{sat,1}}{d_1} & \frac{Y_{user}-Y_{sat,1}}{d_1} & \frac{Z_{user}-Z_{sat,1}}{d_1} & 1 \\ \frac{X_{user}-X_{sat,2}}{d_2} & \frac{Y_{user}-Y_{sat,2}}{d_2} & \frac{Z_{user}-Z_{sat,2}}{d_2} & 1 \\ \frac{X_{user}-X_{sat,3}}{d_3} & \frac{Y_{user}-Y_{sat,3}}{d_3} & \frac{Z_{user}-Z_{sat,3}}{d_3} & 1 \\ \frac{X_{user}-X_{sat,4}}{d_4} & \frac{Y_{user}-Y_{sat,4}}{d_4} & \frac{Z_{user}-Z_{sat,4}}{d_4} & 1 \end{bmatrix}, \tag{2}$$

$$D = [S^T \cdot S]^{-1}, \tag{3}$$

$$GDOP = \sqrt{D_{11} + D_{22} + D_{33} + D_{44}}. \tag{4}$$

Satellites are assumed to be visible when their position has a minimum elevation of 5° from the horizon when viewed from the ellipsoid surface [11], [18]. As more than four satellites may be visible at a particular time, the GDOP is calculated for the best four visible satellites. Figure 2 shows a calculation example for this case.

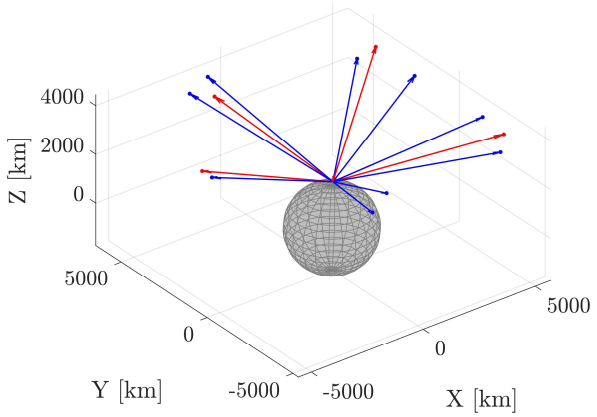


Figure 2. GDOP Calculation for More Than Four Visible Satellites (red: used, blue: also visible)

In the case that less than four satellites are visible, no GDOP can be calculated. With this scheme, the best GDOP achievable is calculated for every surface point for all constellations under consideration.

### *2.2.3 Communication – Reference Link*

A reference link is established for the S- and Ka-Band downlink connections as a basis for subsequent calculations and performance evaluations. The central measure for the link is the signal-to-noise ratio (SNR), which is determined by

$$SNR = P_{R\,[dBm]} - N_{T[dBm]} - M_{[dBm]}, \tag{5}$$

where $P_R$ is the total received power, $N_T$ is the total noise power in the system, and $M$, assumed to be 3 dB, is the link margin. The total noise power takes the form

$$N_T = 10 \log k_B T_{sys} B \ [dBW], \quad (6)$$

where $k_B$ is the Boltzmann constant and $B$ = 5 MHz/100 MHz is the assumed bandwidth for S- and Ka-Band, respectively. $T_{sys}$ is the system noise temperature, which is the sum of both antenna noise temperatures, assumed to be $T_{sys}$ = 120 K/334 K for S- and Ka-Band, respectively. The total received power is calculated through

$$P_R = EIRP_{[dBm]} - L_{T[dB]} + G_{ground[dBi]}, \quad (7)$$

where $EIRP = G_{sat[dBi]} + P_{sat[dBm]}$ is the effective isotropic radiated power (EIRP), $G_{sat}$ is the satellite antenna gain, $P_{sat}$ is the satellite input power, and $G_{ground}$ is the ground antenna gain. The total losses $L_T$ are a sum of the free space loss $L_{FS}$, depointing loss $L_{point}$, scan loss $L_{scan}$, and a system implementation loss $L_{sys}$ = 1.2 dB [19]. The free space loss is calculated through [20]

$$L_{FS} = 20 \log \frac{4\pi d}{c} \ [dB], \quad (8)$$

where $d$ is the distance between the transmitter and receiver, $f$ is the frequency, and $c$ is the speed of light. The depointing loss describes the loss when deviating from the boresight direction and is given by [21]

$$L_{point} = 12 \left(\frac{\theta}{\theta_{3dB}}\right)^2 \ [dB], \quad (9)$$

where $\theta$ is the pointing error and $\theta_{3dB}$ is the beamwidth of the antenna. For phased array antennas, a scan loss describes the reduction in antenna gain when the main antenna lobe is steered with a scan angle $\alpha$. The resulting loss takes the form of [22]

$$L_{scan} = 10 \log (\cos^{1.5}(\alpha)) \ [dB]. \quad (10)$$

For the S- and Ka-Band links, reference antennas are selected for further calculations. The satellite S-Band antenna is a generic nadir-pointing horn antenna with a beamwidth of $\theta_{3dB,S}$ = 25.81°, a gain of $G_{sat,S}$ = 16 dBi and an input power of $P_{sat,S}$ = 100 W. The Ka-Band antenna is an initially nadir-pointing electronically steerable phased array antenna with an $EIRP$ = 79 dBm [23] and is assumed to be steerable up to $\alpha$ = 60°. For simplicity and to allow comparability, a tracking parabolic dish antenna with a diameter of 1 m and an efficiency of 60% is assumed as the ground antenna for both links.

*2.2.4 Communication – Constellation Capacity*

Similar to previous studies [24], [25], this analysis uses a measure of constellation capacity (CC) to investigate the influence of different parameters on the performance of the constellation. However, the theoretical single channel CC introduced in this tradespace analysis, described similarly by Baccelli et al. [16], is a simplified value considering only the link between the satellites and the LS and one active channel per satellite. It neglects the impact of the Earth surface (ES) to Lunar orbit (LO) connection, different possible Lunar surface antenna designs, and aspects such as frequency reuse, multiple access technique, and network architecture, as they are nearly independent of the considered tradespace parameters used in this analysis. Furthermore, the assumptions and parameters of the Lunar user terminal and satellite are kept constant in the reference link to allow for comparability of the results.

The theoretical single-channel CC is calculated by multiplying the theoretically possible data rate per link (calculated via the Shannon-Hartley limit [26]) with the total number of satellites in the constellation

$$CC_{Theo} = B * log_2(1 + SNR) * NOS * NOP, \quad (11)$$

using the SNR calculated for the worst-case reference link. For this case, a general depointing loss of $L_{point}$ = 3 dB and the maximum free space loss (link with the furthest visible satellite from any surface point) is assumed. Therefore, this value does not reflect the effective constellation capacity or constellation throughput as described in other studies [24], [25]. However, it illustrates the dependency of the constellation performance on the variable constellation parameters of SMA, NOS, and NOP.

*2.2.5 Communication – Power Flux Density*

The maximum PFD mapping is introduced to assess the aspect of coverage and LS performance distribution, which is highly dependent on the constellation design and not covered by the theoretical capacity. The evaluation maps the received maximum PFD for each of the 500 surface measurement points, indicating not only the link performance to a given point but also the location dependency of the constellation performance on the surface of the Moon.

For each measurement point in S-Band, the received power of a visible satellite (above 10° elevation) is considered if the surface point is within the nadir pointing 3 dB-cone. For the Ka-Band electronically steerable antennas, each visible satellite (above 10° elevation) is assumed to be pointing at the respective surface location, which requires a maximum of 30° of scan angle for the minimum SMA considered. The received PFD for one point is then determined with [21]

$$PFD = \frac{10^{\frac{EIRP_{[dBW]}-L_{loss[dB]}}{10}}}{4\pi d^2} \text{ [W/m}^2\text{]}. \quad (12)$$

The losses $L_{loss}$ include the actual depointing loss $L_{point}$ for the S-Band connection, and the scan loss $L_{scan}$ for the steerable Ka-Band antenna, respectively. The theoretical maximum PFD for a surface point is then the summation of the PFD from each visible satellite.

Therefore, the maximum PFD value of a surface measurement point reflects the total possible PFD with all visible satellites in the 3 dB cone for S-Band or steering towards the surface point for Ka-Band. It does not reflect the simultaneously received PFD of every measurement point, especially for Ka-Band, but the maximum possible power that could be accessed at a surface point as a sole sink for the constellation. This assumption is made to ensure the comparability of different surface points when considering steered spot beams.

## 3. Tradespace Results and Discussion

This section covers the results of the navigation and communication performance analysis and discusses the impacts of these results on the constellation architecture. Based on a specific weighting of the FOMs, the different constellations are compared, and a set of parameters is selected for further study.

### *3.1 Navigation Performance*

Figure 3 shows the GDOP coverage averaged over the SMA for the different NOP and NOS considered. The results show that the GDOP coverage increases with the total number of satellites in use. This is because more satellites in more planes improve the probability of a favorable constellation of four satellites, giving an optimum GDOP. The dark areas in the plot indicate that the coverage is very low, a result of a low number of visible satellites for these NOP-NOS combinations and, therefore, not enough satellites to calculate a GDOP. In addition, results indicate that a coverage of 100% is difficult to achieve and requires many satellites, although the GDOP coverage scales quickly when the total number of satellites is low.

The optimum way to distribute a given number of satellites around the Moon now becomes the primary consideration. Expanding the previous plot into 3D space, the combinations of NOP and NOS values resulting in a specific minimum coverage at a given SMA can be visualized. The NOP-NOS combinations resulting in a coverage of over 95% with a GDOP < 6 are shown in Figure 4. Results indicate that a higher SMA leads to a lower number of required satellites for a given coverage. This range can be between NOP x NOS = 5 x 3 = 15 and 6 x 5 = 30 satellites needed for the maximum and minimum SMA, respectively.

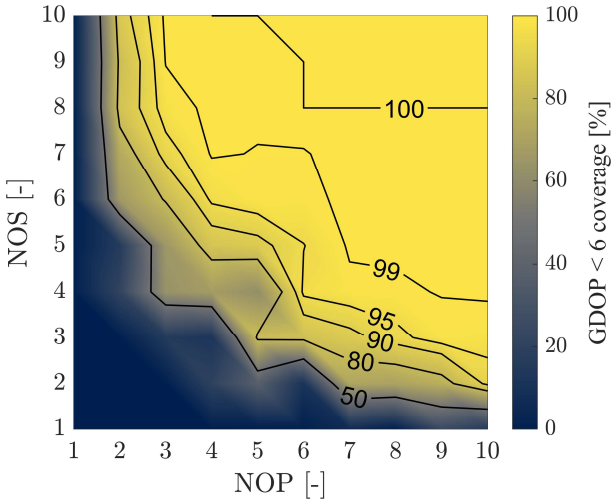

Figure 3. Coverage with GDOP < 6 averaged over SMA

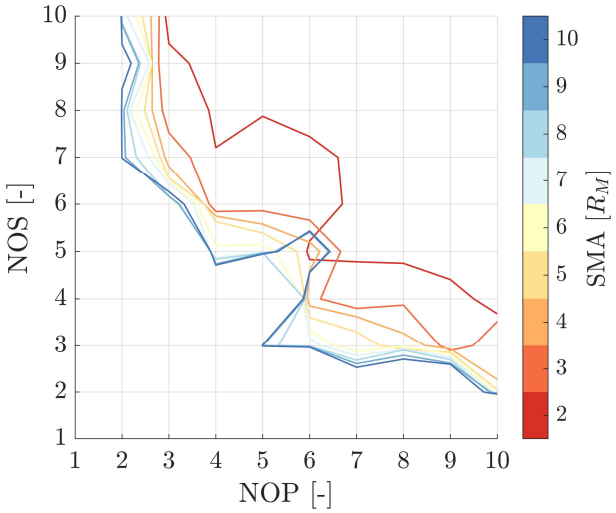

Figure 4. Minimum NOP-NOS combinations for above 95% coverage with GDOP < 6

The results also show an unexpected behavior around the NOP = 6 and NOS = 5 point. This distribution of satellites for the largest SMA leads to a coverage of 91.2% and stems from 44 points barely missing the requirement with GDOPs between 6 and 6.25. These points lie around the equator region of the Moon. Investigating this phenomenon further, it is found that, e.g., the 5 NOP/4 NOS point has a particularly unfavorable GDOP service. With the chosen parameters, especially the Walker constellation and frozen orbit conditions, some points in the equator region achieve very poor GDOP performance (see Figure 5). Because of the minimum elevation considered, these points only see one satellite per plane. Figure 6 shows an example of how the proximity of these visible satellites then creates a particularly unfavorable combination for the GDOP calculation.

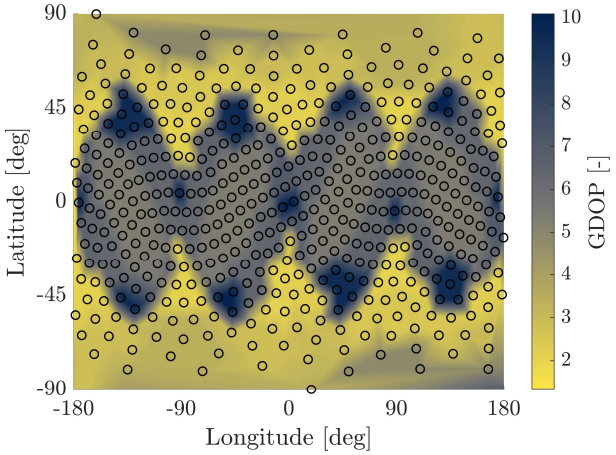


Figure 5. GDOP Ground Map for 9/5/4 (SMA [$R_M$]/NOP/NOS) Configuration

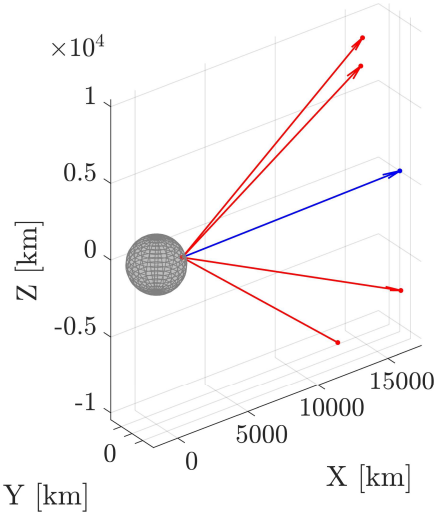


Figure 6. GDOP Calculation Configuration for Exemplary Surface Point for 9/5/4 (SMA [$R_M$]/NOP/NOS) Configuration

From an architectural perspective, increasing the navigation capability of the constellation can be achieved by an increment in the x, y, and z directions, which corresponds to (1) opening a new plane with satellites and changing the RAAN distribution of all planes, (2) adding new satellites to all existing planes, and (3) increasing the SMA of all orbit planes. As Figure 3 and Figure 4 demonstrate, the positive impact of a change depends on the initial starting point. In the bottom half of the NOP-NOS plane, a vertical movement is more beneficial than a horizontal increment. The opposite is the case for the left half of the plane. Increasing the SMA also has a higher impact when moving from lower altitudes.

The impact of adding a new plane of satellites depends on the timing of the decision and is determined by the need for a new dedicated launch for the new satellites. Increasing the SMA for all orbit planes may be achieved by adding a dedicated propulsion system to the satellites. In contrast, adding new satellites to all existing planes may be difficult to achieve but can, in theory, be achieved with a single launch [27]. However, the initial deployment of the constellation may also be easier for a higher number of satellites delivered to fewer orbit planes, which in turn favors an initial constellation on the left side of the NOS-NOP plane in Figure 3.

### *3.2 Communication Performance*

The communication performance evaluation is aimed at generating simple performance measures dependent on the same variable parameters as the GDOP. This is done to allow for the combined assessment of both navigation and communication services and to illustrate the effect of these parameters for this specific frozen orbit Walker constellation. Both the navigational and the communication performance are highly dependent on the SMA and satellite distribution in the constellation. The impact of SMA, NOP, and NOS on both communication and navigation performance, however, differ and, with respect to SMA, are entirely contrary.

The results for CC for both S- and Ka-Band, shown in Figure 7 and Figure 10, primarily illustrate that the capacity measure scales linearly with the total number of satellites and according to the inverse square law for the SMA as a result of the free space loss. This also holds for the average PFD for all connected measurement points, illustrated in Figure 8 and Figure 11. However, for very low SMAs and lower numbers of satellites, not all surface points have access to a satellite simultaneously. This reflects that low and small constellations cannot provide global coverage and 100% access time for the entire surface. Figure 9 illustrates that at least 12 or 21 satellites at a SMA of 4/5 Lunar radii are required to achieve 100% access time and global coverage for the chosen S-Band antenna. The effect is less pronounced for the Ka-Band as the steerable phased array can access the visible surface with only limited scan loss compared to high depointing losses of the nadir-facing S-Band antenna.

Figure 13 depicts the PFD measure mapped to the surface grid of the Moon and illustrates the performance distribution for the conceptual design described in Section 4. As a result of the necessary relatively low inclinations for the frozen orbit condition, less PFD, about -3 dB compared to the Lunar equator, is available in the polar region. As this region is of primary interest, the constellation performance evaluation and design must compensate for this fact.

Another aspect that needs consideration is access during Earth eclipse times when satellites do not have a line of sight to Earth. Whether a surface location on the far side

has continuous access to a satellite with a line of sight to Earth is also dependent on the SMA, NOS, NOP, and satellite design (not considering inter-satellite links). Geometric analysis can show that under the condition of 100% access time and coverage, with a minimum SMA of about 4 $R_M$, a constellation can provide a minimum elevation angle of 10° to a satellite with a direct line of sight to Earth at all times. Therefore, inter-satellite link capability is not necessarily required and, therefore, not considered for this analysis.

In conclusion, the evaluation of CC and PFD indicates minimal required parameters for the chosen frozen orbit constellation design to achieve the goal of global coverage and 100% access time. Furthermore, they reinforce the fact that a higher number of satellites is necessary to keep a specific performance for increasing the SMA.

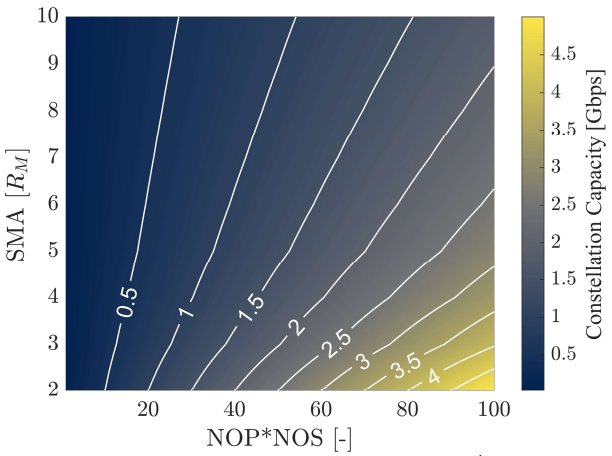


Figure 7. S-Band Constellation Capacity*

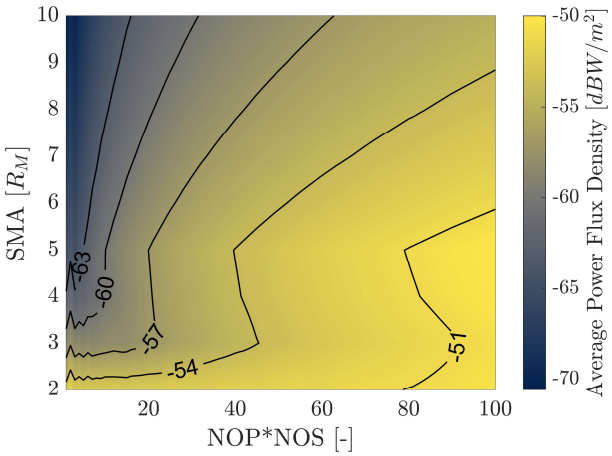


Figure 8. S-Band Average Power Flux Density of Connected Surface Points*

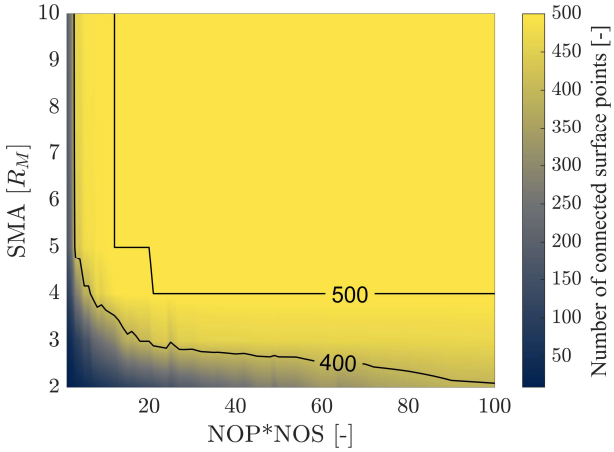


Figure 9. Number of Connected Surface Points for S-Band Connection*

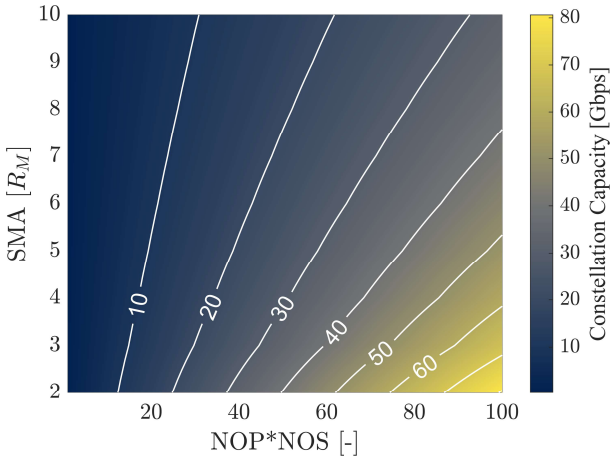


Figure 10. Ka-Band Constellation Capacity*

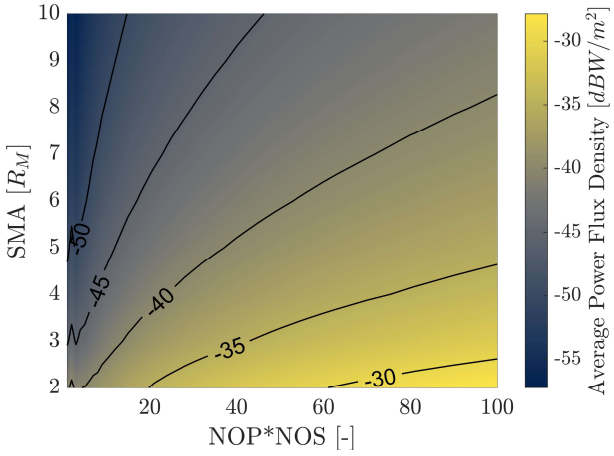


Figure 11. Ka-Band Average Power Flux Density of Connected Surface Points*

* The results for configurations not covered in the design vector are derived with linear interpolation.

### *3.3 Combined Performance*

The combined performance assessment of the navigation and communication performance shall select the parameters used for the conceptual design. For this selection, some wanted parameters need to be established for an adequate GDOP and link performance. As mentioned in Section 2.1, the navigation performance is determined by the surface coverage with a GDOP < 6. For the S-Band FOMs, a $CC_S$ of 500 Mbps and a coverage with a minimum theoretical $PFD_S$ of -60 dBW/m$^2$ are selected. For Ka-Band, a $CC_{Ka}$ of 10 Gbps and $PFD_{Ka}$ of -43 dBW/m$^2$ are used. The coverage assigns a direct FOM from 0 to 100%, whereas the CC assigns a value from 0 to 100% based on the percentage of fulfillment of the target. The communication performance is summarized into one value based on equal weighting of the four communication FOMs. This total communication value is then weighed equally against the navigation performance to yield a final combined FOM. It needs to be noted that these weights may shift when weighing the GDOP coverage higher than the communication FOM, e.g., if communication assets on the surface and in orbit may be utilized to ease the required communication performance of this NAVCOM constellation.

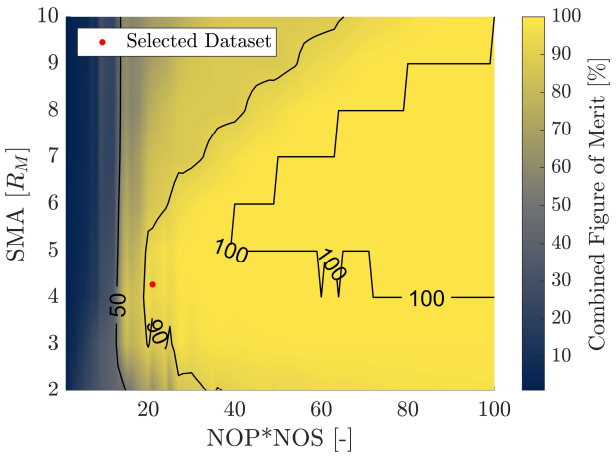


Figure 12. Combined Figure of Merit

Figure 12 shows the combined navigation and communication FOM. In general, constellations with less than 12 satellites are unable to provide enough performance for the NAVCOM service as they fail to achieve a FOM > 50. In addition, constellations with the two smallest SMA cannot achieve global GDOP and S-Band coverage. Optimal performance is achieved with a minimum of 39 satellites with a SMA > 4-5 $R_M$. However, sending this number of satellites is unrealistic from an economic perspective of primarily scientific mission focus on the Moon. Therefore, when considering a combined FOM of 90%, the number of required satellites decreases drastically, with a total as low as 20 satellites achieving this threshold. Therefore, a 21-satellite constellation with NOP = 3, NOS = 7, and a SMA of 7434.8 km [10] is selected and indicated with a red mark in Figure 12. This configuration achieves a GDOP coverage of 97.2%, a $CC_S$ of 658 Mbps, and $PFD_S$ > -60 dBW/m$^2$ coverage of 99.8% in S-Band, shown in Figure 13, where just one surface point is not sufficiently covered at this time. In Ka-Band, a $CC_{Ka}$ of 12 Gbps and $PFD_{Ka}$ > -43 dBW/m$^2$ coverage of 97.8% can be achieved. Therefore, its combined FOM of 98.3% places this configuration beyond the edge of the 90% FOM line.

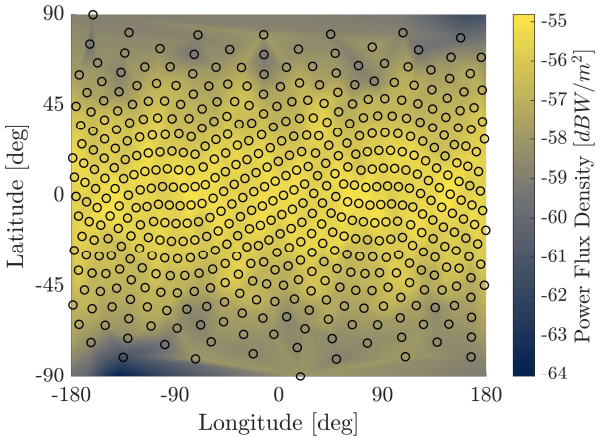


Figure 13. S-Band Power Flux Density Map for Conceptual Design

## 4. Conceptual Design

This section presents a conceptual design for a Lunar NAVCOM constellation based on the findings of the previous chapters. First, the underlying mission requirements are presented. Secondly, a mission architecture and a potential operations concept are presented. Finally, the detailed navigation and communication architectures are discussed further, along with a potential satellite bus design.

### *4.1 Mission Requirements and Assumptions*

The conceptual design for a Lunar NAVCOM constellation is derived based on key mission requirements. The architecture aims to provide navigation services with a GDOP < 6 for more than 95% of the LS and communication services in S- and Ka-Band at more than 97% of the LS. In addition, the constellation shall serve a lifetime of 10 years for a launch no earlier than 2031.

### *4.2 Mission Architecture and Concept of Operations*

As derived from the tradespace analysis, the constellation is comprised of 21 satellites in a 3-plane, 7-satellites-per-plane configuration. In addition, one extra satellite per plane is included to provide redundancy, resulting in a total of 24 satellites. The spare satellites are kept in a

lower parking orbit for synchronization with the operational orbit. The relevant orbit parameters are given in Table 2.

Table 2. Orbit Parameters of Conceptual Design

| Variable | Value |
|---|---|
| SMA | 7434.8 km [10] |
| $SMA_{park}$ | 6100 km |
| ECC | 0 |
| INC | 39.67 deg |
| RAAN | 0, 120, 240 deg |

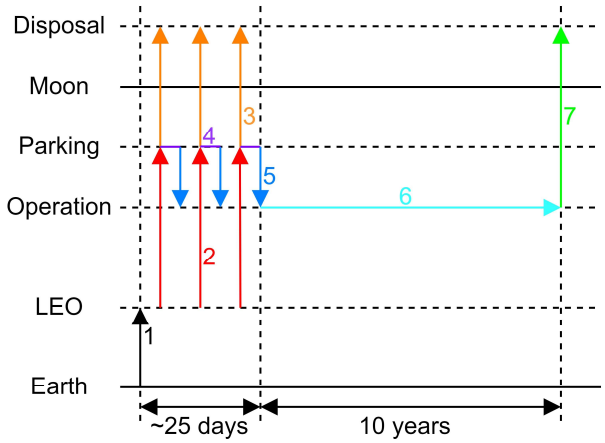


Figure 14. Concept of Operations

The Concept of Operations for the constellation is depicted in Figure 14. Initially, 24 satellites are launched with a single SpaceX Starship launch vehicle. Here, the satellites are divided into groups of eight per delivery upper stage for a total of three delivery vehicles deployed from the Starship payload fairing. Over 25 days, the three batches of satellites are then delivered to the parking orbit in the respective plane of the operational orbit (2). After deploying the satellites, the delivery vehicles will immediately perform another burn to achieve a heliocentric orbit for disposal (3). After checkouts of the satellite systems (4), each satellite will stay in the parking orbit for phasing with the intended position in the operational orbit. Then, seven of eight satellites will perform a Hohmann transfer to achieve the operational orbit (5). Nominal operations can commence with all 21 operational satellites in the correct orbit (6). After the ten-year lifespan, the spacecraft will be injected into a heliocentric orbit for disposal (7).

For a derivation of the maximum mass per satellite, the 150 t payload capability of the SpaceX Starship launch vehicle [28] is equally distributed among the three delivery vehicles. Assuming payload and structure coefficients of 0.366 and 0.01, respectively, paired with a specific impulse of 382 s and a total maximum $\Delta v$ of 4091 m/s for the delivery vehicle, a maximum of 12.69 t can be transported to each orbit plane, resulting in a maximum mass of 1792 kg per satellite to the parking orbit.

### *4.3 Navigation Architecture and Payload*

The navigation service is based on an analogous concept to that of existing GNSS systems. Therefore, each satellite transmits a navigation message containing its respective satellite time, ephemeris, time correction data, system status, and almanac. The format of the navigation message is identical to that of the GPS navigation message [17]. The navigation signal is transmitted between 2483.5 and 2500.0 MHz in S-Band, following the Space Frequency Coordination Group guidelines for satellite radio navigation services to the Lunar orbit and surface [29]. The navigation signal employs code division multiple access with Binary Phase Shift Keying (BPSK) as the modulation scheme. This enables the utilization of existing receiver technology [30].

The navigation payload design is based on the Galileo satellite navigation payload model [31], with the adaptation that Rubidium Atomic Frequency Standards (RAFS) are used as atomic clocks exclusively. In addition to the RAFS, the navigation payload comprises a Clock Monitoring and Control Unit (CMCU), a Frequency Generation Upconverter Unit (FGUU), and a Navigation Signal Generation Unit (NSGU). Table 3 presents an overview of the navigation payload components, including their respective mass and average power consumption.

Table 3. Navigation Payload Components

| Component | Unit | Power | Mass | Ref |
|---|---|---|---|---|
| RAFS | 3 | ≤ 35 W | 3.4 kg | [32] |
| CMCU | 1 | ≤ 21 W | 5.2 kg | [33] |
| FGUU | 1 | ≤ 22 W | 7.6 kg | [34] |
| NSGU | 1 | ≤ 27 W | 12 kg | [35] |

The CMCU is responsible for synthesizing the frequencies of the master clock and the two additional backup clocks. In the event of a misalignment of the clocks, the CMCU initiates a switchover, designating a spare clock as the new master clock. The FGUU converts the signal into a reference clock signal for the NSGU, which receives the satellite position information from the onboard computer and the reference clock signal as input and modulates this information into the navigation message, which is then up-converted by the FGUU into their transmission frequency. The transceiver then amplifies the navigation signal and transmits it via the antenna. Figure 15 illustrates the configuration of the navigation payload.

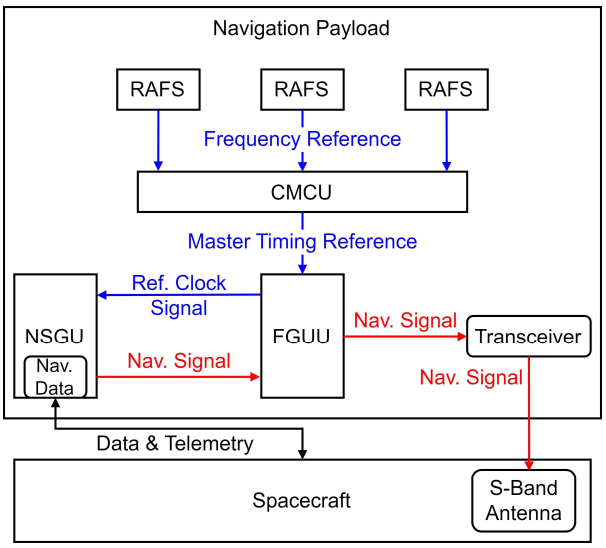

Figure 15. Navigation Payload Architecture

The time synchronization of the satellites' atomic clocks is achieved using inter-constellation cross-links. This method allows for the determination of a single reference clock time. The cross-link will permit satellites to autonomously identify potential clock errors as they communicate their onboard time across the constellation, thereby enabling the detection of any clock misalignments.

The determination of the satellites' orbits is conducted by three beacon stations situated on the LS. The precise location of the beacon stations is known. Each beacon system comprises an atomic clock and transmits a navigation signal. The satellites determine their position by receiving navigation messages from all three beacons. The dispersion of the beacons on the LS is not addressed in further detail in this paper. Nevertheless, the satellites are required to receive all three navigation signals transmitted by the beacon stations simultaneously.

*4.4 Communication Architecture and Payload*

Each satellite of the proposed concept has seven operational antennas. One parabolic 1.2 m Ka-Band antenna for the link towards Earth, a high gain Electronic Steerable Phase Array antenna for a Ka-Band link towards the Moon, a fixed horn antenna for the same link in S-Band, and a patch antenna on each side of the satellite for the inter-satellite link in S-Band. The inter-satellite links are integrated to allow time coordination between the satellites. Furthermore, two omnidirectional S-Band antennas are installed to transmit and receive Telemetry, Tracking, and Command (TT&C) data from Earth during the Launch and Early Operations phase.

For the link calculation, S-Band 34 m ground stations similar to the Deep Space Network (DSN) [36] are assumed. For Ka-Band, 10 m parabolic antennas are assumed. Regarding the LS user, a 1 m parabolic antenna with tracking is assumed. This assumption is made to simplify calculations and allow comparability. Furthermore, it is chosen to neglect the detailed analysis of various possible surface use cases and user terminal scenarios described in the LunaNet standard, as well as the impact of network architecture, frequency reuse, and multiple access to focus on the satellite conceptual design and demonstrate the considerations of the tradespace analysis.

As required by LunaNet, Ka-Band is utilized for the link towards Earth because of higher possible bandwidths due to congestion in lower bands [12]. The Ka-Band ground station network on Earth is assumed to allow close to constant availability, requiring several distributed locations for line of sight to the Moon and redundancy, e.g., in case of outages or storms severely impacting Ka-Band capability. In general, and especially for the downside of high rain attenuation in the Ka frequency band, techniques such as adaptive ground station switching, signal routing, uplink power control, and bandwidth control are assumed. In addition to Ka-Band, an S-Band link is utilized for the LO-LS/LS-LO link as required for LunaNet and Lunar Search and Rescue applications [12]. As a consequence, the S-Band LS-LO link will be transferred to Ka-Band for the LO-ES path. In contrast to the high data throughput Ka-Band link, the S-Band link is primarily intended for low bandwidth operation, such as with smaller, low-power, nearly omnidirectional ground antennas.

As the constellation is planned to support future human and robotic exploration, the communication services must fulfill the expected needs of those missions. A possible minimum case of the system is defined similarly to Noreen et al. [37]: a base at the Lunar South Pole, which is inhabited by 12 astronauts, with 20 rovers and four transport vehicles nearby. The total data rate requirement for the up- and downlink is calculated based on the assumed use cases shown in Table 4. The given use cases are only examples to estimate and illustrate possible data rate requirements. In order to account for satellite TT&C transmissions, 8 kbps are added to the reliability links to Earth [8]. For the navigation link, 250 bps are needed [17]. In summary, about 100 Mbps Ka-Uplink and 140 Mbps in Ka-Downlink between Earth and Moon, 644 kbps in S-Uplink, and 170 kbps in S-Downlink for the Satellite-Moon link are required. Additionally, 18.25 kbps are required for the inter-satellite link. However, possible limiting maximum symbol rate scenarios for BPSK modulation of 2-5 Msps and a maximum of 2 Gsps per link are already stated for LunaNet [12]. The document, however, does not mention in which scenarios and with which LS terminals these rates should be achieved.

This implies that significantly higher data rates than initial minimum scenarios could be required. Therefore, this concept aims for hundreds of Mbps in a single link and a constellation capacity in the gigabit range with the assumed 1 m LS antennas.

The link budget calculation described in the following section is calculated under the simplification of a single link per satellite utilizing full possible bandwidths still allowed by the LunaNet standard.

Table 4. Data Rate Requirements for Different Use Cases

| User | Data | Rate per Channel | # of Channels |
|---|---|---|---|
| **Reliable S-Band Channels** | | | |
| Uplink | | | |
| Astronauts | Speech | 10 kbps | 12 |
| | Engineering | 2 kbps | 12 |
| Rover, Transport, Base | Engineering | 20 kbps | 25 |
| Downlink | | | |
| Astronauts | Speech | 10 kbps | 12 |
| Rover, Transport, Base | Digital Commands | 2 kbps | 25 |
| **High Data Rate Ka-Band Channels** | | | |
| Uplink | | | |
| Astronauts, Rover, Transport, Base | Hyperspectral Imaging, Radar, HDTV | 100 Mbps | 1 |
| Downlink | | | |
| Astronauts | Video | 1.5 Mbps | 12 |
| | HQ-Audio | 128 kbps | 12 |
| | HDTV | 20 Mbps | 1 |

Link Budget calculations are performed equivalently to the reference link described in Section 2.2.3; however, now considering the full ES-LS forward and return link. A summary of the intermediate values and calculations is shown in Table 5. Frequencies and bandwidths are taken from LunaNet [12], although not the entire bandwidth is usable with 1 m terminals. The worst-case maximum distances for the LS-LO link are calculated with the evaluation tool of the tradespace analysis, and the Earth-Moon distance is assumed with their average distance. G/T values are calculated for the satellite and Moon surface terminals using exemplary values of noise temperatures from Wertz et al. [38], while the Earth ground stations G/T are calculated based on Schwerdtfeger [39]. For antennas facing the Moon, additional noise temperatures because of Lunar flux are taken into account [40]. Values for additional losses, such as implementation loss, rain attenuation, and depointing losses, are calculated according to Maral [21]. In conjunction with the simplification of a single channel per satellite, the bandwidth is maximized to the limit of LunaNet frequency allocation and the limit of link stability, for example, for BPSK of about 9.6 C/N, assuming a bit error rate of $10^{-5}$ [38]. This is done under the assumption of neglecting aspects of multiple access, spectral efficiency, and network architecture. These aspects are highly dependent on specific use cases and network architecture, which are not the focus of this analysis and conceptual design. This design is meant to be a possible design based on the results of the tradespace analysis and a starting point for further necessary investigation of optimal and more detailed network architectures.

Table 5. Link Budget Summary

| **Forward** | | | |
|---|---|---|---|
| **Parameter** | **Ka ES-LO** | **Ka LO-LS** | **S LO-LS** |
| C-Freq. [GHz] | 23 | 23.3 | 2.08 |
| EIRP [dBW] | 95.42 | 49 | 36.01 |
| G/T [dB/K] | 18.8 | 20.3 | 3.76 |
| Total Losses [dB] | 242.47 | 201.04 | 183.63 |
| **C/N0 [dBHz]** | **99.74** | **96.86** | **84.73** |
| **Return** | | | |
| **Parameter** | **Ka LO-ES** | **Ka LS-LO** | **S LS-LO** |
| C-Freq. [GHz] | 26.25 | 27.25 | 2.245 |
| EIRP [dBW] | 74.17 | 66.1 | 45.21 |
| G/T [dB/K] | 42.09 | 12.0 | -9.99 |
| Total Losses [dB] | 245.19 | 210.4 | 184.96 |
| **C/N0 [dBHz]** | **99.68** | **96.31** | **78.85** |

The results of the individual links are then combined for both the concepts of a transparent and regenerative satellite design and the satellite throughputs multiplied by the number of satellites to calculate the theoretical maximum constellation capacity. The results of the possible throughputs are shown in Table 6. In conclusion, the regenerative satellite design generally allows for higher data rates, mission flexibility, and more sophisticated and efficient network architectures at the cost of system complexity and development costs [21]. Considering the benefits, this concept chooses a regenerative design resulting in estimated possible single forward data rates of 375 Mbps in Ka-Band and 22.5 Mbps in S-Band. In the return link, data rates of 337 Mbps and 6 Mbps are calculated for Ka- and S-Band, respectively. In total, this gives a theoretical maximum constellation capacity of 8.35 Gbps and 7.21 Gbps in forward and return paths, respectively.

Table 6. Possible Single-Link Data Rates

| **Forward** | | | |
|---|---|---|---|
| | **Transparent** | **Regenerative** | **Regenerative** |
| **Parameter** | **Ka** | **Ka** | **S** |
| Tot. C/N0 [dBHz] | 95.05 | 96.86 | 84.73 |
| Bandwidth [MHz] | 330 | 500 | 30 |
| Tot. C/N [dB] | 9.87 | 9.87 | 9.96 |
| Mod. | BPSK3/4 | BPSK3/4 | BPSK3/4 |
| **Rate [Mbps]** | **247.5** | **375.0** | **22.5** |
| **Return** | | | |
| | **Transparent** | **Regenerative** | **Regenerative** |
| **Parameter** | **Ka** | **Ka** | **S** |
| Tot. C/N0 [dBHz] | 94.66 | 96.31 | 78.85 |
| Bandwidth [MHz] | 300 | 450 | 8 |
| Tot. C/N [dB] | 9.89 | 9.77 | 9.82 |
| Mod. | BPSK3/4 | BPSK3/4 | BPSK3/4 |
| **Rate [Mbps]** | **225.0** | **337.5** | **6.0** |

*4.5 Satellite Bus Design*

The satellite bus houses all components required for the operation of the satellite payloads throughout the mission. The pre-phase A design of the satellite includes major components and their placement around the satellite bus, but shall not be representative of a flight-ready design.

The configuration of a satellite, shown in Figure 16, Figure 17, and Figure 18, features a central load-bearing frame inside which the heaviest components, namely propellant tanks, batteries, and reaction wheels, are placed. This configuration minimizes the moment of inertia and the loads on the main structure during launch. Most of the payloads and essential hardware components are mounted on a ”payload ring” around the midplane of the main structure. This allows minimal cable routing within the bus and outside elements. A star sensor is mounted to the main truss on the starboard side. Six side panels are mounted on all sides of the spacecraft to give a cuboid appearance and house smaller components, like the radiators, smaller antennas, thrusters, and sun sensors.

All satellites utilize a hydrazine monopropellant blow-down propulsion system. Twelve small thrusters and two larger thrusters are used for reaction wheel desaturation and the required orbital maneuvers, respectively. For power generation and storage, the bus uses two 5 $m^2$ roll-out solar panels similar to those used on the Double Asteroid Redirect Test mission [41] and two battery packs with a total storage capacity of 13940 Wh at the beginning of the mission. The overall mass budget of a satellite, based on current best estimates and a 20% mass margin, is shown in Table 7.

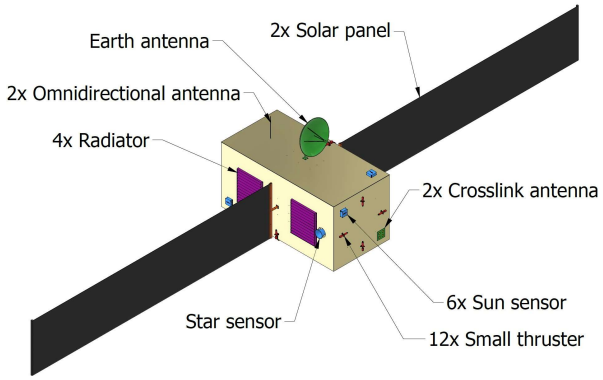


Figure 16. Satellite Bus Outside View

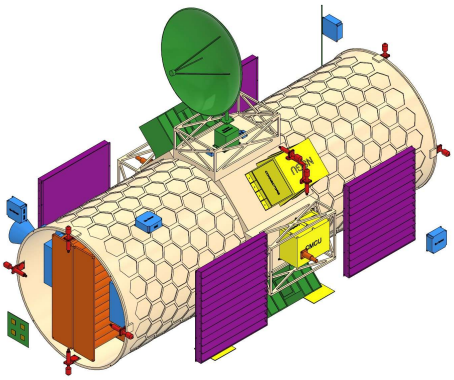

Figure 17. Satellite Bus Inside View

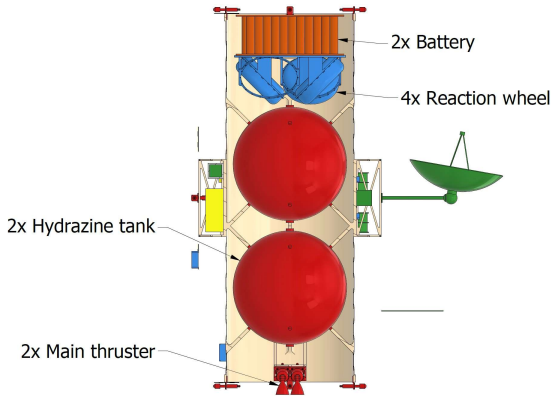


Figure 18. Satellite Bus Sliced View

Table 7. Satellite Mass Breakdown (all in kg)

| Component | Level 2 | Level 1 |
|---|---|---|
| 1.0 Payload | | 42.71 |
| 1.1 Navigation | 42.71 | |
| 2.0 Spacecraft Bus (dry) | | 694.65 |
| 2.1 Attitude Determination and Control | 78.93 | |
| 2.2 Propulsion | 67.48 | |
| 2.3 Onboard Computer | 10.13 | |
| 2.4 Communication | 27.21 | |
| 2.5 Electrical Power System | 167.12 | |
| 2.6 Structure | 311.03 | |
| 2.7 Thermal | 32.75 | |
| 3.0 Spacecraft Dry Mass | | 737.36 |
| 4.0 Propellant | | 315.78 |
| 5.0 Pressurant | | 8.36 |
| 6.0 Loaded Mass | | 1061.50 |
| 7.0 Launch Adapter | | 100.00 |
| 8.0 Boosted Mass | | 1161.50 |
| 9.0 Margin | | 630.50 |
| 10.0 Launcher Capability | | 1792.00 |

## 5. Conclusion and Future Work

This paper performed a tradespace analysis on three major design parameters for a Lunar NAVCOM constellation in circular frozen orbits. The performance analysis for the GDOP showed that the navigation capability improves with the SMA and an increase in the number of satellites. In contrast, the communication performance, assessed with the CC and PFD for the S- and Ka-Band downlink connection, decreases with the SMA but shows a similar improvement with an increase in the number of satellites. Furthermore, the GDOP also showed a dependency on the distribution of a given number of satellites onto the orbit planes, while the PFD coverage in S-Band showed that a minimum SMA of around 4 Lunar radii is required to get close to 100% coverage. Based on FOMs of the navigation and communication performance and a combined performance evaluation, a 21-satellite constellation with 3 NOP and 7 NOS is selected for further analysis.

Based on this selection, a more detailed conceptual design is carried out for this constellation launched with a single SpaceX Starship. This includes the mission, navigation and communication architectures as well as a more detailed satellite bus design sized for a Lunar South Pole station reference scenario.

This paper should serve as a starting point for more detailed investigations into Lunar NAVCOM constellations utilizing circular frozen orbits. Further work should include more architecture selections, including whether to include crosslinks or a relay satellite in the Lagrange points, as well as the incorporation of the Earth link into the tradespace. In addition, more orbital parameters can be varied, e.g., to obtain elliptical orbits. A more detailed analysis should be conducted on the impact of the tradespace variables on the spacecraft design, including the power and mass budget. Lastly, a thorough cost analysis is not performed in this paper. Still, it can give more insights into the profitability and feasibility of a combined Lunar NAVCOM constellation from an economic point of view.

## Acknowledgment

The author expresses his sincere gratitude to the ESA Academy Conference Student Sponsorship Programme and the Bund der Freunde der TUM e.V. for sponsoring the main- and co-authors' attendance at the IAC. We would also like to thank Dr. Jürgen Letschnik and Victor Martius for their valuable input.

## References

[1] National Aeronautics and Space Administration, "NASA's Lunar Exploration Program Overview," Washington, D.C., NP-2020-05-2853-HQ, Sep. 2020. Accessed: May 30, 2024. [Online]. Available: https://www.nasa.gov/wp-content/uploads/2020/12/artemis_plan-20200921.pdf

[2] S. Creech, J. Guidi, and D. Elburn, "Artemis: An Overview of NASA's Activities to Return Humans to the Moon," in *2022 IEEE Aerospace Conference (AERO)*, Big Sky, MT, USA: IEEE, Mar. 2022, pp. 1–7. doi: 10.1109/AERO53065.2022.9843277.

[3] H. D. Lopes *et al.*, "GNSS-Based Navigation for Lunar Missions," in *27th International Technical Meeting of the Satellite Division of The Institute of Navigation (ION GNSS+ 2014)*, Tampa, FL: The Institute of Navigation, Sep. 2014. Accessed: May 20, 2024. [Online]. Available: https://www.researchgate.net/publication/275882232_GNSS-Based_Navigation_for_Lunar_Missions

[4] A. Delépaut *et al.*, "Use of GNSS for lunar missions and plans for lunar in-orbit development," *Adv. Space Res.*, vol. 66, no. 12, pp. 2739–2756, Dec. 2020, doi: 10.1016/j.asr.2020.05.018.

[5] V. Capuano, "GNSS-Based Navigation for Lunar Missions," Ph.D. Thesis, EPFL, Lausanne, 2016. doi: https://doi.org/10.5075/epfl-thesis-7130.

[6] A. Grenier *et al.*, "Positioning and Velocity Performance Levels for a Lunar Lander using a Dedicated Lunar Communication and Navigation System," *Navig. J. Inst. Navig.*, vol. 69, no. 2, p. navi.513, 2022, doi: 10.33012/navi.513.

[7] M. Flanegan *et al.*, "NASA's Lunar Communication and Navigation Architecture," in *SpaceOps 2008*

*Conference*, Heidelberg, Germany: American Institute of Aeronautics and Astronautics, May 2008. doi: 10.2514/6.2008-3589.

[8] K. Hamera, T. Mosher, M. Gefreh, R. Paul, L. Slavkin, and J. Trojan, "An Evolvable Lunar Communication and Navigation Constellation Concept," in *2008 IEEE Aerospace Conference*, Big Sky, MT, USA: IEEE, Mar. 2008, pp. 1–20. doi: 10.1109/AERO.2008.4526326.

[9] J. Thompson, H. Haygood, and M. Kezirian, "Design and Analysis of Lunar Communication and Navigation Satellite Constellation Architectures," in *AIAA SPACE 2010 Conference & Exposition*, Anaheim, California: American Institute of Aeronautics and Astronautics, Aug. 2010. doi: 10.2514/6.2010-8644.

[10] F. Pereira and D. Selva, "Exploring the Design Space of Lunar GNSS in Frozen Orbit Conditions," in *2020 IEEE/ION Position, Location and Navigation Symposium (PLANS)*, Portland, OR, USA: IEEE, Apr. 2020, pp. 444–451. doi: 10.1109/PLANS46316.2020.9110202.

[11] F. Pereira, P. M. Reed, and D. Selva, "Multi-Objective Design of a Lunar GNSS," *Navig. J. Inst. Navig.*, vol. 69, no. 1, p. navi.504, 2022, doi: 10.33012/navi.504.

[12] "LunaNet Interoperability Specification Document," LN-IS V004, Sep. 2022. Accessed: Sep. 08, 2024. [Online]. Available: https://www3.nasa.gov/sites/default/files/atoms/files/lunanet_interoperability_specification_version_4.pdf

[13] J. G. Walker, "Satellite Constellations," *J. Br. Interplanet. Soc.*, vol. 37, p. 559, Dec. 1984.

[14] D. Folta and D. Quinn, "Lunar Frozen Orbits," in *AIAA/AAS Astrodynamics Specialist Conference and Exhibit*, Keystone, Colorado: American Institute of Aeronautics and Astronautics, Aug. 2006. doi: 10.2514/6.2006-6749.

[15] T. Nie and P. Gurfil, "Lunar frozen orbits revisited," *Celest. Mech. Dyn. Astron.*, vol. 130, no. 10, p. 61, Oct. 2018, doi: 10.1007/s10569-018-9858-0.

[16] F. Baccelli, S. Candel, G. Perrin, and J.-L. Puget, "Large Satellite Constellations: Challenges and Impact," Académie des sciences, Mar. 2024. doi: 10.62686/3.

[17] J.-M. Zogg, Ed., *GPS: essentials of satellite navigation ; compendium ; theory and principles of satellite navigation, overview of GPS/GNSS systems and applications*. Thalwil: U-Blox, 2009.

[18] F. D. Moorefield, "Global Positioning System Standard Positioning Service Performance Standard," Department of Defense, Washington, D.C., Apr. 2020. Accessed: Sep. 07, 2024. [Online]. Available: https://www.gps.gov/technical/ps/2020-SPS-performance-standard.pdf

[19] W.-J. Lee, K.-K. Cho, D.-W. Yoon, and K.-M. Hyun, "Design and Performance Analysis of Downlink in Space Communications System for Lunar Exploration," *J. Astron. Space Sci.*, vol. 27, no. 1, pp. 11–20, Mar. 2010, doi: 10.5140/JASS.2010.27.1.011.

[20] J. R. Wertz, D. F. Everett, and J. J. Puschell, Eds., *Space Mission Engineering: The New SMAD*. in Space technology library, no. 28. Torrance: Microcosm Press, 2011.

[21] G. Maral, M. Bousquet, and Z. Sun, *Satellite Communications Systems: Systems, Techniques and Technology*, 5th ed. Chichester, West Sussex, U.K: John Wiley, 2009.

[22] R. J. Mailloux, *Phased array antenna handbook*, Third edition. Norwood, MA: Artech House, 2018.

[23] BAE Systems, Inc., "Ka-Band SATCOM Antennas." 2024. Accessed: Sep. 08, 2024. [Online]. Available: https://www.baesystems.com/en-media/upload-File/20240416183358/1573701746678.pdf

[24] I. Del Portillo, B. G. Cameron, and E. F. Crawley, "A technical comparison of three low earth orbit satellite constellation systems to provide global broadband," *Acta Astronaut.*, vol. 159, pp. 123–135, Jun. 2019, doi: 10.1016/j.actaastro.2019.03.040.

[25] N. Pachler, I. Del Portillo, E. F. Crawley, and B. G. Cameron, "An Updated Comparison of Four Low Earth Orbit Satellite Constellation Systems to Provide Global Broadband," in *2021 IEEE International Conference on Communications Workshops (ICC Workshops)*, Montreal, QC, Canada: IEEE, Jun. 2021, pp. 1–7. doi: 10.1109/ICCWorkshops50388.2021.9473799.

[26] C. E. Shannon, "A Mathematical Theory of Communication," *Bell Syst. Tech. J.*, vol. 27, no. 3, pp. 379–423, 623=656, Jul. 1948.

[27] S. Carletta, "A Single-Launch Deployment Strategy for Lunar Constellations," *Appl. Sci.*, vol. 13, no. 8, p. 5104, Apr. 2023, doi: 10.3390/app13085104.

[28] Space Exploration Technologies Corp., "Starship." Accessed: Aug. 01, 2024. [Online]. Available: https://www.spacex.com/vehicles/starship/

[29] Space Frequency Coordination Group, "Radio Communication Frequency Allocations and Sharing in the Lunar Region," SFCG-31, 2012. Accessed: Aug. 24, 2024. [Online]. Available: https://cwe.ccsds.org/sls/docs/SLS-RFM/Meeting%20Materials/2011/Fall/PCOM/AI_Lunar_Radio%20Comm%20Frequency%20Plan_notrackchange.pdf

[30] P. J. G. Teunissen and O. Montenbruck, Eds., *Springer Handbook of Global Navigation Satellite Systems*. Cham: Springer International Publishing, 2017. doi: 10.1007/978-3-319-42928-1.

[31] D. Felbach, D. Heimbuerger, P. Herre, and P. Rastetter, "Galileo payload 10.23 MHz master clock generation with a Clock Monitoring and Control Unit (CMCU)," in *IEEE International Frequency Control Symposium and PDA Exhibition Jointly with the 17th European Frequency and Time Forum, 2003. Proceedings of the 2003*, Tampa, Fl, USA: IEEE, 2003, pp. 583–586. doi: 10.1109/FREQ.2003.1275156.

[32] Safran, "RAFS." Feb. 2023. Accessed: Aug. 24, 2024. [Online]. Available: https://safran-navigation-timing.com/wp-content/uploads/2023/03/RAFS-SAFRAN-Datasheet.pdf

[33] Airbus Defense & Space, "CMCU - Clock Monitoring and Control Unit." 2014. Accessed: Aug. 24, 2024. [Online]. Available: https://satsearch.co/products/airbus-defence-and-space-clock-monitoring-and-control-unit-cmcu

[34] Kongsberg, "FGUU." Sep. 2014. Accessed: Aug. 24, 2024. [Online]. Available: https://www.kongsberg.com/kmagazine/2014/9/board-galileo/

[35] Thales Alenia Space Italy, "TRIS NSGU." Jun. 2012. Accessed: Aug. 24, 2024. [Online]. Available: https://www.thalesgroup.com/sites/default/files/database/d7/asset/document/TRIS_NSGU-092012.pdf

[36] S. D. Slobin, T. T. Pham, and C. Chang, "34-m BWG Stations Telecommunications Interfaces," Jet Propulsion Laboratory, DSN No. 810-005, 104, Rev. N, Jun. 2021. Accessed: Aug. 25, 2024. [Online]. Available: https://deep-space.jpl.nasa.gov/dsndocs/810-005/104/104N.pdf

[37] G. K. Noreen *et al.*, "Integrated network architecture for sustained human and robotic exploration," in *2005 IEEE Aerospace Conference*, Big Sky, MT, USA: IEEE, 2005, pp. 1266–1285. doi: 10.1109/AERO.2005.1559417.

[38] J. R. Wertz and W. J. Larson, Eds., *Space mission analysis and design: SMAD III*, 3. ed., 10. print. in Space technology library, no. 8. Hawthorne, Calif: Microcosm Press [u.a.], 2008.

[39] R. Schwerdtfeger, *Microwave Reflector Antenna Design Concepts and Techniques*. 2011.

[40] D. D. Morabito, "Lunar Noise-Temperature Increase Measurements at S-Band, X-Band, and Ka-Band Using a 34-Meter-Diameter Beam-Waveguide Antenna," *Interplanet. Netw. Prog. Rep.*, vol. 42–166, Aug. 2006, Accessed: Sep. 19, 2024. [Online]. Available: https://tmo.jpl.nasa.gov/progress_report/42-166/166C.pdf

[41] J. M. Owen, M. E. DeCoster, D. M. Graninger, and S. D. Raducan, "Spacecraft Geometry Effects on Kinetic Impactor Missions," *Planet. Sci. J.*, vol. 3, no. 9, p. 218, Sep. 2022, doi: 10.3847/PSJ/ac8932.